JOURNAL OF GUIDANCE, CONTROL, AND DYNAMICS
Vol. 16, No. 2, March-April 1993

Q-Markov Covariance Equivalent Realization and its Application to Flexible Structure Identification

Ketao Liu* and Robert E. Skelton†
Purdue University, West Lafayette, Indiana 47907

The Q-Markov covariance equivalent realization algorithm is applied to NASA's Minimast structure to identify state-space models for the purpose of designing closed-loop controllers, and laboratory test results are shown for the identification and for the closed-loop performance. The paper also presents for the first time a deterministic formulation of covariance parameters from a pulse response, a stochastic formulation of Markov parameters from a white-noise response, and a simple Q-Markov covariance equivalent realization formulation. This requires only pulse laboratory tests or only white-noise laboratory tests to generate Q-Markov covariance equivalent realizations.

I. Introduction

IN physical problems, one never has an exact mathematical model of the system. We begin our discussions here without any presumption about either the parameters or the order of the system,

$$x(k+1) = Ax(k) + Dw(k) \tag{1a}$$

$$y(k) = Cx(k) + Hw(k) \tag{1b}$$

That is, the parameters (A,D,C,H) are unknown, where $w(k) \in \Re^{n_w}$ is the known input, $y(k) \in \Re^{n_y}$ is the known output response, and $x \in \Re^{n_x}$ is the state of unknown dimension n_x. Under these conditions we seek an approximation of Eqs. (1) given only the input/output data $w(k)$ and $y(k)$. There are many approximation methods, but most divide into one of two categories: those that seek a least-squares fit to some scalar measure of the system data, and those that seek to match (exactly) certain specific (but not all) properties of the system. Hankel norm methods[1-6] fall into the first category and Q-Markov covariance equivalent realizations (Q-Markov covers) fall into the second category.[7-16] To put other differences into perspective, we cite some known properties of any linear system, Eq. (1).

Let $W>0$, and define a matrix X by

$$X \triangleq \sum_{i=0}^{\infty} A^i DWD^* A^{i*} \tag{2a}$$

where the asterisk denotes matrix transpose (or complex conjugate transpose if the matrix is complex). If A is stable, then X satisfies

$$X = AXA^* + DWD^* \tag{2b}$$

Define "Markov" parameters H_i and "covariance" parameters R_i by

$$H_0 \triangleq H, \qquad H_i \triangleq CA^{i-1}D, \qquad i = 1,2,\ldots \tag{3a}$$

$$R_i \triangleq CA^i XC^* + H_i WH^*, \qquad i = 0,1,2,\ldots \tag{3b}$$

At this point, we attach neither deterministic nor stochastic interpretation to H_i and R_i.

A Q-Markov cover is a state-space realization of Eq. (1) which matches R_i and H_i for $i = 0,1,2,\ldots,Q-1$. Using frequency domain techniques, Mullis and Roberts[10] and Inouye[11] find reduced-order models using first- and second-order information (Markov and covariance parameters.) Similar ideas were developed in the time domain (the Q-Markov cover approach).[12-14]

We shall hereafter further shorten the acronym Q-Markov cover to simply QMC. To illustrate the significance of the parameters H_i and R_i, note that if $x(0) = 0$, the response to any input is

$$y(k) = \sum_{i=0}^{k} H_i w(k-i) \tag{4}$$

For a single-input/single-output system, $2n_x$ Markov parameters are required to completely define the system. For example, a third-order system can be uniquely determined (hence, the system is completely defined) by the first six Markov parameters $(H_1,H_2,H_3,H_4,H_5,H_6)$. On the other hand, the system can be completely defined by specifying fewer than six Markov parameters if some covariance parameters R_i are also specified. Hence, the six parameters $(H_1,H_2,H_3,H_4,R_0,R_2)$ uniquely define the system. It has been shown that[14] a strictly proper transfer function of order n_x is completely matched by a QMC with Q equal to the smallest integer equal to or larger than $\bar{Q} = (4/3)n_x$. For the preceding third-order system $(\bar{Q} = 4)$, suppose the system parameters are completely unknown. Then the realization problem may proceed by measuring either 1) six Markov parameters or 2) four Markov parameters (H_1,H_2,H_3,H_4) and two covariance parameters (R_0,R_2). We show how to measure this later. This use of covariance data is the main difference in the point of view between the Hankel norm methods (which work only with Markov parameters) and QMC methods. The choice of $Q = 4$ in the QMC would attempt (with success) to match all four parameters (R_0,R_1,R_2,R_3), but this is more than the required number, raising the question of whether extra, unnecessary computations are present in the QMC algorithm. This extra matching comes for free and does not burden the computation since the R_i and H_i are not independent pieces of data. All of the relationships between the Markov and covariance parameters (H_i,R_i) appear in Ref. 14 and this is the key to the QMC method. Now suppose for the third-order system only (H_1,H_2,R_0,R_1) are known. Then the QMC with $Q = 2$ generates a lower-order approximation that matches (H_1,H_2,R_0,R_1,R_2).

Normally, H_i has the deterministic meaning, Eq. (4), and R_i has a stochastic meaning

$$R_i = \lim_{k\to\infty} Ey(k+i)y^*(k)$$

Received May 15, 1990; revision received Jan. 15, 1991; accepted for publication June 2, 1992.

*Visiting Assistant Professor, School of Aeronautics and Astronautics; currently Research Associate, Massachusetts Institute of Technology, Space Engineering Research Center, Room 37-351, 77 Massachusetts Avenue, Cambridge, MA 02139.

†Professor, School of Aeronautics and Astronautics.

with white noise for $w(k)$. Prior QMC algorithms[15] required two laboratory tests to generate both sets of data. However, in this paper, a new QMC algorithm is presented which operates only from pulse response data or from white-noise response data. This provides both a completely deterministic QMC theory and also a completely stochastic theory.

The QMC is not unique. For discrete-time systems, Anderson and Skelton[14] and King et al.[15] developed algorithms to generate all Q-Markov covers (starting with only Q-Markov parameters, H_i and covariance parameters R_i). This data set appears to require both pulse input experiments (to get the Markov parameters H_i) and white-noise input experiments (to get the covariance parameters R_i), and that is the intent of the algorithm in Ref. 15. This paper reduces the number of required laboratory tests by one-half. We will show how to obtain a QMC using only pulse inputs or using only noise inputs. The new algorithms generate all Q-Markov covers for the system, Eqs. (1). The method requires only two decisions by the user: the specification of Q and zero threshold ϵ for the determination of rank of a data matrix.

Quite often in aerospace problems, the prediction or control of multiple output rms values is important. Matching R_0 will accomplish this, since $(y_i)_{\text{rms}} = \sqrt{R_{0_{ii}}}$. Hence, any QMC with $Q \geq 1$ is a lower-order realization of the full system, but nonetheless one that guarantees matching of the rms values of each of the n_y outputs y_i, $i = 1,2,\ldots,n_y$. Since accurate rms prediction and control is our objective in the Minimast experiment, the QMC is the most natural choice for our identification experiments. Matching of both a subset of the H_i and the R_i is clearly a prima facie attractive basis for identification. The tasks of matching only the H_i or only the R_i has been considered separately.[7-9]

The Hankel approximation methods beginning with Ho and Kalman[1] and Kung[2] are least-squares methods in the sense that the norm (squared) of {the Hankel matrix from the data} minus {the Hankel matrix of the realization} is minimized. However, the most significant feature of the Hankel methods is the existence of an upper bound on the error of the transfer function.[17,18] The QMC theory promises no such bound. This upper bound depends only on the singular values truncated in the singular value decomposition (SVD) of the Hankel matrix. If only "small" singular values are deleted, the transfer function error will be "small." Of course, with an a priori truncation of the Hankel matrix of data (Markov parameters) as in Refs. 3 and 4, these desirable theoretical features may be lost.

Anderson[9] described the class of models that preserve the entire sequence R_i, $i = 0,1,\ldots,\infty$. However, Markov parameters are not preserved. Hence, these realizations[9] may replace a nonminimal phase system by a minimum-phase representation, since transient properties are ignored. One of the most important features of flexible structures is that these systems are usually nonminimum phase. Nonminimum-phase systems are much more difficult to control. It would be virtually impossible to design a good controller for a nonminimum-phase system using a minimum-phase model for control design, even if a magnitude error bound is known for the transfer function (a feature of Hankel methods). Hankel methods can produce a minimum-phase realization for a nonminimum-phase system. The missing information here is phase information. This has led some researchers in Hankel methods[6] to seek to add phase information in the realization, but these approaches are quite complicated.

When developing models for control design, it is extremely important to have a realization method that preserves the nonminimal-phase feature of the system at least to an acceptable degree of approximation. The Q-Markov cover possesses this feature quite easily and naturally (by adjustment of Q). Hence, if the step response initially goes negative before it eventually goes positive, the QMC will follow (up to $k = Q-1$) this nonminimum-phase trajectory.

The philosophy of the Q-Markov cover is to choose Q (the length of the matched portion of the response, and the number of autocorrelations that are matched). This matches certain deterministic and also certain stochastic properties of the system. The QMC theory guarantees stability of the realization and the explicit parameterization of all realizations (of a given order) with the stated properties. In the QMC parameterization, this freedom is characterized by an arbitrary unitary matrix[14,15] and could be used to get additional properties beyond matching Markov and covariance parameters.

The preceding discussion relates to the theoretical properties of the methods, under the assumption of error-free measurements as in Eqs. (1). In the presence of measurement errors (noise, bias, etc.), none of the theories hold exactly, and one cannot argue for a "best" methodology. Hence, for some time to come it will be useful to continue to research both QMC and Hankel methodologies, because they are distinctly different approaches.

The paper is organized as follows. Section II gives both deterministic and stochastic interpretations of H_i and R_i. Section III presents a simpler deviation of the QMC than is heretofore available. Section IV discusses practical aspects when the measurements are corrupted by noise, and gives the QMC algorithm. Section V describes the Minimast system and the identification experiment. Section VI discusses a 40th-order model and the control design. Section VII offers some conclusions.

II. Deterministic and Stochastic Formulations of Both Markov and Covariance Parameters

In this section, deterministic formulations of covariance parameters and stochastic formulations of Markov parameters are introduced to show how to generate a QMC from either pulse or white-noise excitation.

Assume now that the system, Eq. (1), is excited by a single-pulse input. We define $y(j,k)$ and $x(j,k)$ to be the output and state vectors at time k in response to a single-pulse excitation in the jth input channel only [zero input in all other channels and zero initial conditions, $x(0) = 0$]. Write the single-pulse input $w(j,k)$ as

$$w(j,k) \triangleq \begin{bmatrix} 0 \\ \vdots \\ w_j \\ \vdots \\ 0 \end{bmatrix} \delta_{ok} \tag{5a}$$

where δ_{ok} is the Kroneker delta and w_j is the magnitude of the single pulse. Define the matrix of magnitudes of $w(j,k)$ as

$$W_I \triangleq \text{diag}[w_1^2 \quad w_2^2 \quad \cdots] \tag{5b}$$

Then, define

$$X_I(d,i) \triangleq \sum_{j=1}^{n_w} \sum_{k=0}^{d} x(j,k+i)x^*(j,k) \tag{6a}$$

$$Y_I(d,i) \triangleq \sum_{j=1}^{n_w} \sum_{k=0}^{d} y(j,k+i)y^*(j,k) \tag{6b}$$

$$Y_k \triangleq \left[y(1,k), y(2,k), \ldots, y(n_w,k)\right] \tag{6c}$$

We shall call

$$Y_I(\infty,i) \triangleq \lim_{d\to\infty} Y_I(d,i)$$

and

$$X_I(\infty,i) \triangleq \lim_{d\to\infty} X_I(d,i)$$

the deterministic "autocorrelation" parameters of output and state. Y_k is the impulse response matrix at time k of a multi-input and multi-output system. One can show by straight-

forward substitutions that if the matrices W and W_I in Eqs. (2b) and (5b) all have the same numerical value,

$$W = W_I \tag{7}$$

then X, R_i, and H_i have the following deterministic meaning,

$$\left.\begin{aligned} X &= X_I(\infty,o) && && (8a)\\ R_i &= Y_I(\infty,i) && i=0,1,2,\ldots && (8b)\\ H_i &= Y_i W^{-1/2} && i=0,1,2,\ldots && (8c)\end{aligned}\right\}\text{deterministic}$$

For the stochastic meaning of R_i consider the output response sequence $\{y(k)\}$ of system, Eq. (1), in response to a zero mean white-noise sequence $\{w(k)\}$, with steady-state covariance matrix W_E:

$$W_E = \lim_{k\to\infty} E\{w(k)w^*(k)\} \tag{9}$$

The steady-state autocorrelations of $y(k)$ and $x(k)$ and the steady-state cross correlation R_i^{yw} between $y(k)$ and $w(k)$ are defined by

$$R_i^x \triangleq \lim_{k\to\infty} E\{x(k+i)x^*(k)\} \tag{10a}$$

$$R_i^y \triangleq \lim_{k\to\infty} E\{y(k+i)y^*(k)\} \tag{10b}$$

$$R_i^{yw} \triangleq \lim_{k\to\infty} E\{y(k+i)w^*(k)\} \tag{10c}$$

It is also straightforward to show that if matrices W and W_E in Eqs. (2b) and (9) have the same numerical value

$$W = W_E \tag{11}$$

then the following facts lend stochastic meaning to both Markov and covariance parameters.

$$\left.\begin{aligned} X &= R_0^x && && (12a)\\ R_i &= R_i^y && i=0,1,2,\ldots && (12b)\\ H_i &= R_i^{yw}W^{-1} && i=0,1,2,\ldots && (12c)\end{aligned}\right\}\text{stochastic}$$

Equalities (12a–12c) are well known in statistics when input $w(k)$ is a stationary stochastic process. Equality (8c) basically states that Markov parameters form the unit-pulse response of the system, which is also a well-known fact. The proofs of equalities (8a) and (8b) are shown in Ref. 22. These results, Eqs. (8) and (12), interpret Markov parameters and covariance parameters in terms of both stochastic and deterministic properties of a system. Hence, in the stochastic interpretation, a Q-Markov cover is a state-space realization matching the first Q output-input cross-correlation parameters R_i^{yw} and output covariance parameters R_i^y of a system. In the deterministic interpretation, a Q-Markov cover matches the first Q pulse response samples $[y(i,k),\ 1\le i\le n_w,\ 0\le k\le Q-1]$ and the first Q deterministic output autocorrelation parameters $[Y_I(\infty,i),\ 0\le i\le Q-1]$.

The preceding results allow the identification algorithm presented in this paper to be used when either white noise or pulse inputs are applied to the system. The identification problem to be solved can be stated as follows.

Identification Problem

Given either set of data matrices $\{W_E,\ R_i^y,\ R_i^{yw},\ i=0,1,\ldots,Q-1\}$ or $\{W_I,\ Y_I(\infty,i),\ Y_i,\ i=0,1,\ldots,Q-1\}$, find all minimal and stable Q-Markov covers that match the data (R_i^y, R_i^{yw}) or $[Y_I(\infty,i),\ Y_i]$, $i=0,1,\ldots,Q-1$. ■

We can now begin the QMC development using only the matrices denoted R_i, H_i, where these matrices are formed from the raw data $(R_i^y,\ R_i^{yw},\ W_e)$ or $[Y_I(\infty,i),\ Y_i,\ W_I]$. Hence, with the help of Eqs. (8) and (12), the preceding identification problem reduces to the following realization problem.

Realization Problem

Given matrices $\{R_i, H_i, i=0,1,\ldots,Q-1\}$, find all minimal and stable Q-Markov covers that match the data. ■

III. Simpler Formulation of the Q-Markov Cover

Here we discuss the formulation of the QMC from the given data R_i and H_i, $i=0,1,\ldots,Q-1$. The results presented in this section simplify the formulation of the discrete Q-Markov cover given in Ref. 15. Define the following matrices $\boldsymbol{R}_Q$, $\boldsymbol{H}_Q$ with Toeplitz structure by using the first Q-Markov parameters H_i and covariance parameters R_i (from laboratory tests)

$$\boldsymbol{R}_Q \triangleq \begin{bmatrix} R_0 & R_1^* & \cdots & R_{Q-1}^* \\ R_1 & R_0 & \cdots & \\ \cdots & & \ddots & \\ R_{Q-1} & & \cdots & R_0 \end{bmatrix} \quad \boldsymbol{R}_Q \in \mathbb{R}^{[n_y Q]\times[n_y Q]} \tag{13a}$$

$$\boldsymbol{H}_Q \triangleq \begin{bmatrix} H_0 & 0 & \cdots & 0 \\ H_1 & H_0 & \cdots & 0 \\ \vdots & \vdots & \ddots & \vdots \\ H_{Q-1} & H_{Q-2} & \cdots & H_0 \end{bmatrix} \quad \boldsymbol{H}_Q \in \mathbb{R}^{[n_y Q]\times[n_y Q]} \tag{13b}$$

From the actual (but of course unknown) system (A,C,D) generating the data, define matrices $\boldsymbol{O}_Q$, $\boldsymbol{D}_Q$, $\boldsymbol{M}_Q$ by

$$\boldsymbol{O}_Q \triangleq \begin{bmatrix} C \\ CA \\ \vdots \\ CA^{Q-1} \end{bmatrix} \in \mathbb{R}^{n_y Q\times n_x} \tag{13c}$$

$$\boldsymbol{D}_Q \triangleq \boldsymbol{O}_Q X \boldsymbol{O}_Q^* \in \mathbb{R}^{n_y Q\times n_y Q} \tag{13d}$$

$$\boldsymbol{M}_Q \triangleq \boldsymbol{O}_{Q-1} D = \begin{bmatrix} H_1 \\ H_2 \\ \vdots \\ H_{Q-1} \end{bmatrix} \in \mathbb{R}^{n_y(Q-1)\times n_w} \tag{13e}$$

The following is the key to QMC theory. The proof appears in Ref. 14.

For any linear system, Eq. (1), the response data $\boldsymbol{R}_q$, $\boldsymbol{H}_q$ are related to the actual model parameters (C,A,D,H) by the relationship

$$\boldsymbol{D}_Q = \boldsymbol{R}_Q - \boldsymbol{H}_Q \bar{W} \boldsymbol{H}_Q^* \tag{14}$$

where $\bar{W} \triangleq \operatorname{diag}[W \quad W \quad \cdots \quad W] \in \mathbb{R}^{n_w Q\times n_w Q}$.

The significance of Eq. (14) is that the model parameters, Eq. (13d), appearing on the left-hand side of Eq. (14) can be computed from test data, Eqs. (13a) and (13b), appearing on the right-hand side of Eq. (14). This is accomplished by finding a matrix factor of the right-hand side of Eq. (14). Note that this procedure (using the data matrix $\boldsymbol{D}_Q$) is quite different from Hankel approaches, which instead work entirely with the Hankel matrix formed from the Markov parameters H_i.

The computation of Q-Markov covers starts from the data matrices $\boldsymbol{D}_Q$, $\boldsymbol{M}_Q$, and H_0. Define a full column rank matrix factor of $\boldsymbol{D}_Q$ as $\boldsymbol{P}_Q$. Hence,

$$\boldsymbol{D}_Q = \boldsymbol{P}_Q \boldsymbol{P}_Q^*, \qquad \boldsymbol{P}_Q \in \mathfrak{R}^{n_y Q \times \hat{n}_x}, \qquad \boldsymbol{P}_Q^* \boldsymbol{P}_Q > 0 \tag{15a}$$

where $\hat{n}_x = \text{rank}(\boldsymbol{D}_Q)$. Partition the $\boldsymbol{P}_Q$ matrix as

$$\boldsymbol{P}_Q = \begin{bmatrix} P_0 \\ P_1 \\ \vdots \\ P_{Q-1} \end{bmatrix}, \quad P_i \in \mathfrak{R}^{n_y \times n_x}, \quad i = 0,1,\ldots,Q-1 \tag{15b}$$

To complete the realization, define

$$\boldsymbol{P} \triangleq \begin{bmatrix} P_0 \\ \vdots \\ P_{Q-2} \end{bmatrix}, \qquad \bar{\boldsymbol{P}} \triangleq \begin{bmatrix} P_1 \\ \vdots \\ P_{Q-1} \end{bmatrix}, \qquad \boldsymbol{P}, \bar{\boldsymbol{P}} \in \mathfrak{R}^{n_y(Q-1) \times n_x} \tag{15c}$$

Then we have the following results to generate all Q-Markov covers from a given set of data $\{\boldsymbol{R}_Q, \boldsymbol{M}_Q, H_0\}$ defined in Eqs. (13) and (14). Let $V_p \in \mathfrak{R}^{\hat{n}_x \times (\hat{n}_x - n)}$ denote a unitary basis for the nullspace of $\boldsymbol{P}$. Let $V_{\bar{p}} \in \mathfrak{R}^{(\hat{n}_x + n_w) \times (\hat{n}_x - r)}$ denote a unitary basis for the nullspace of $[\bar{\boldsymbol{P}} \quad \boldsymbol{M}_Q]$. Then the SVD of $\boldsymbol{P}$ (of rank r) and $[\bar{\boldsymbol{P}} \quad \boldsymbol{M}_Q]$ may be written in the form

$$\boldsymbol{P} = U_p \begin{bmatrix} \Sigma_p & 0 \\ 0 & 0 \end{bmatrix} \begin{bmatrix} V_{p_1}^* \\ V_p^* \end{bmatrix}, \quad [\bar{\boldsymbol{P}} \quad \boldsymbol{M}_Q] = U_p \begin{bmatrix} \Sigma_p & 0 \\ 0 & 0 \end{bmatrix} \begin{bmatrix} V_{\bar{p}_1}^* \\ V_{\bar{p}}^* \end{bmatrix} \tag{16}$$

Using these notations, we have the following result.

Theorem: All minimal Q-Markov covers of a stable system, Eq. (1), generating data $\{\boldsymbol{R}_Q, \boldsymbol{M}_Q, H_0\}$ can be parameterized by the following equations

$$[\hat{A} \quad \hat{D}] = \boldsymbol{P}^+ [\bar{\boldsymbol{P}} \quad \boldsymbol{M}_Q] + V_p U V_{\bar{p}}^* \begin{bmatrix} I & 0 \\ 0 & W^{-1/2} \end{bmatrix} \tag{17a}$$

$$\hat{C} = P_0, \qquad \hat{H} = H_0 \tag{17b}$$

where $U \in \mathfrak{R}^{(\hat{n}_x - r) \times (\hat{n}_x + n_w - r)}$ is an arbitrary row unitary matrix ($UU^* = I$), and where $\boldsymbol{P}$, $\bar{\boldsymbol{P}}$, $\boldsymbol{M}_Q$, V_p, $V_{\bar{p}}$ are defined in Eqs. (13e), (15), (16), and $r = \text{rank}(\boldsymbol{P})$. All of the Q-Markov covers, Eq. (17), are stable and exist for any value of $Q \geq 1$. ■

The proof is omitted for brevity, and can be found in Ref. 22.

Remark: Since nonsingular coordinate transformations affect neither Markov nor covariance parameters, the total set of all QMCs are given by $\{T^{-1}\hat{A}T, T^{-1}\hat{D}, \hat{C}T, \hat{H}\}$, where T is arbitrary nonsingular and $(\hat{A}, \hat{D}, \hat{C})$ are parameterized by Eqs. (17) in terms of the free parameter U.

The following corollary states the condition for a unique Q-Markov cover.

Corollary: If $\boldsymbol{P}$ is full column rank matrix, the Q-Markov cover is unique (to within a coordinate transformation) and is given by

$$\hat{A} = \boldsymbol{P}^+ \bar{\boldsymbol{P}}, \qquad \hat{C} = P_0, \qquad \hat{D} = \boldsymbol{P}^+ \boldsymbol{M}_Q, \qquad \hat{H} = H_0 \tag{18}$$

■

The proof appears in Ref. 22. This concludes our discussion on the theory of Q-Markov covers.

IV. Practical Aspects of Q-Markov Cover Computation

To apply Q-Markov cover theory for identification, we can replace R_i and H_i in the data matrix $\boldsymbol{D}_Q$ by either R_i^y and R_i^{yw} in the case of white-noise inputs, or by $Y_I(\infty, i)$ and Y_i in the case of pulse inputs, according to Eqs. (8) and (12). If the input $w(k)$ is ergodic, we can compute R_i^y, R_i^{yw}, and W_I by averaging a finite number of data samples

$$R_i^y(d,\tau) = \frac{1}{d} \sum_{k=\tau}^{d+\tau-1} y(k+i)\, y^*(k) \tag{19a}$$

$$R_i^{yw}(d,\tau) = \frac{1}{d} \sum_{k=\tau}^{d+\tau-1} y(k+1)\, w^*(k) \tag{19b}$$

$$W_E(d,\tau) = \frac{1}{d} \sum_{k=\tau}^{d+\tau-1} w(k) w^*(k) \tag{19c}$$

where parameter τ is the time length required for the system to reach steady state. We recommend that data record length d be selected at least four times the parameter τ.

In the case of pulse inputs, $Y_I(\infty, i)$ can be approximated by $Y_I(d,i)$ in Eq. (6b), but we require $d \gg Q$ and the data segment $y(j,k)$, $k > d$ should be below the measurement noise level, since the theory presumes a stable system and no measurement noise, hence $y(j,\infty) = 0$. Measurement errors and computational errors are always present, and since they are not accounted for in the QMC theory, the Markov and covariance parameters will not be matched exactly. So it is impossible to guarantee quantitatively that this approach will be better than any other, but we are encouraged by numerical results to date.

The crucial step in the identification process is determining the rank of $\boldsymbol{D}_Q$. We have from the singular value decomposition,

$$\boldsymbol{D}_Q = P_Q \Lambda P_Q^* \tag{20}$$

where P_Q is a unitary matrix and Λ is a diagonal matrix of singular values of $\boldsymbol{D}_Q$. No singular values in the computed matrix Λ will be exactly zero. We therefore set $\epsilon > 0$ (the zero threshold).

It is possible to set ϵ too large and too small. This is argued as follows. Suppose the singular values are arranged in the Λ matrix in a descending order

$$\Lambda = \begin{bmatrix} \hat{\Lambda} & 0 \\ 0 & \tilde{\Lambda} \end{bmatrix}, \qquad \hat{\Lambda} \in \mathfrak{R}^{\hat{n}_x \times \hat{n}_x} \tag{21a}$$

and the singular values in $\hat{\Lambda}$ are larger than ϵ, and the singular values in $\tilde{\Lambda}$ are smaller than ϵ. We then truncate Λ to $\hat{\Lambda}$.

$$P_Q = [\hat{P}_Q, \tilde{P}_Q], \qquad \hat{P}_Q \in \mathfrak{R}^{n_y(Q-1) \times \hat{n}_x} \tag{21b}$$

where $\hat{n}_x$ is the number of singular values in $\hat{\Lambda}$ and $\hat{\Lambda}$, $\hat{P}_Q$ are the matrices remaining after truncation. Then we compute $\boldsymbol{P}_Q$ in Eq. (15b) by

$$\boldsymbol{P}_Q = \hat{P}_Q \sqrt{\hat{\Lambda}}, \qquad \boldsymbol{P}_Q \in \mathfrak{R}^{n_y(Q-1) \times \hat{n}_x} \tag{21c}$$

If one deletes only the singular values of $\boldsymbol{D}_Q$ that are zero (which the noise-free theory of the preceding section would dictate), one may keep too much of the undesired noise features in the identified model. Therefore, certain averaging or approximating measures should be built into the identification algorithm. Selection of ϵ to a proper value larger than zero is one mechanism for creating the averaging or approximating effect.

We cannot set Q too high due to size restrictions on the dimension of a matrix that can be reliably factored numerically. Hence, the user's selection of Q is limited only by the dimension for which the SVD of a symmetric matrix ($\boldsymbol{D}_Q$) is reliable. If Q is selected too small (a small set of Markov and

covariance parameters are matched) and measurements are noisy, the realization algorithm is bound to produce an unsatisfactory model. It is advisable to set the Q large (up to its computational bound) and select ϵ to a value which will produce a sufficient averaging effect. Up to now however, the choice of ϵ is determined by studying the distribution of the singular values of the $\boldsymbol{D}_Q$ matrix. The precise quantification of the effect of the choice of Q and ϵ on the identification results is still an open question.

Q-Markov Cover Algorithm

Step 1: Set Q and d parameters.

Step 2: Compute R_i and H_i, $i=0,1,\ldots,Q-1$, and W from experimental data.

Stochastic case: White-noise input. Set τ parameter.

$$R_i = R_i^y(d,\tau) \quad H_i = R_i^{yw}(d,\tau)W_I^{-1}(d,\tau), \quad i=0,1,\ldots,Q-1$$

$$W = W_I(d,\tau)$$

Deterministic case: Pulse inputs

$$R_i = Y_I(d,i) \qquad H_i = Y_i W^{-1/2}, \qquad i=0,1,\ldots,Q-1$$

$$W = W_I = \operatorname{diag}[w_1^1 \quad w_2^2 \quad \ldots \quad w_{n_w}^2]$$

where w_j is the magnitude of the jth channel's pulse

Step 3: Form the $\boldsymbol{R}_Q$, $\boldsymbol{M}_Q$, $\boldsymbol{H}_Q$, and $\boldsymbol{D}_Q$ matrices.

$$\boldsymbol{R}_Q = \begin{bmatrix} R_0 & R_1^* & \cdots & R_{q-1}^* \\ R_1 & R_0 & \cdots & \\ \cdots & \cdots & \cdots & \cdots \\ R_{q-1} & \cdots & \cdots & R_0 \end{bmatrix}$$

$$\boldsymbol{H}_Q = \begin{bmatrix} H_0 & 0 & \cdots & 0 \\ H_1 & H_0 & \cdots & \\ \cdots & \cdots & \cdots & \\ H_{q-1} & H_{q-2} & \cdots & H_0 \end{bmatrix}, \qquad \boldsymbol{M}_Q = \begin{bmatrix} H_1 \\ H_2 \\ \vdots \\ H_{q-1} \end{bmatrix}$$

$$\boldsymbol{D}_Q = \boldsymbol{R}_Q - \boldsymbol{H}_Q \bar{W} \boldsymbol{H}_Q^*$$

where $\bar{W} = \operatorname{diag}[W \quad W \quad \ldots \quad W]$.

Step 4: Form $\boldsymbol{P}_Q$ matrix. Singular value decomposition of $\boldsymbol{D}_Q$. Select ϵ after examining the singular value distribution (a plot is helpful).

$$\boldsymbol{D}_Q = [\hat{P}_Q, \tilde{P}_Q] \begin{bmatrix} \hat{\Lambda} & 0 \\ 0 & \tilde{\Lambda} \end{bmatrix} \begin{bmatrix} \hat{P}_Q^* \\ \tilde{P}_Q^* \end{bmatrix}, \qquad \hat{\Lambda} \in \mathfrak{R}^{\hat{n}_x \times \hat{n}_x}$$

Set: $\boldsymbol{P}_Q = \hat{P}_Q \hat{\Lambda}^{1/2}$.

Step 5: Form $\boldsymbol{P}$, $\bar{\boldsymbol{P}}$, and $V_p U V_{\hat{p}}$ matrices.

1) Partition $\boldsymbol{P}_Q$.

$$\boldsymbol{P}_Q = \begin{bmatrix} P_0 \\ P_1 \\ \vdots \\ P_{Q-1} \end{bmatrix}, \qquad P_i \in \mathfrak{R}^{n_y \times \hat{n}_x}, \qquad i=0,1,\ldots,Q-1$$

2) Form $\boldsymbol{P}$ and $\bar{\boldsymbol{P}}$.

$$\boldsymbol{P} = \begin{bmatrix} P_0 \\ \vdots \\ P_{Q-2} \end{bmatrix}, \qquad \bar{\boldsymbol{P}} = \begin{bmatrix} P_1 \\ \vdots \\ P_{Q-1} \end{bmatrix}$$

3) Singular value decomposition of $\boldsymbol{P}$ and $[\bar{\boldsymbol{P}} \quad \boldsymbol{M}_Q]$.

$$\boldsymbol{P} = \begin{bmatrix} U_{p_1} & U_{p_2} \end{bmatrix} \begin{bmatrix} \Sigma_p & 0 \\ 0 & 0 \end{bmatrix} \begin{bmatrix} V_{p_1}^* \\ V_p^* \end{bmatrix}$$

$$[\bar{\boldsymbol{P}} \quad \boldsymbol{M}_Q] = \begin{bmatrix} U_p & U_{p_2} \end{bmatrix} \begin{bmatrix} \Sigma_p & 0 \\ 0 & 0 \end{bmatrix} \begin{bmatrix} V_{\hat{p}_1}^* \\ V_{\hat{p}}^* \end{bmatrix}$$

Step 6: Compute $\hat{A}$, $\hat{C}$, $\hat{D}$, and $\hat{H}$.

$$\hat{A} = \boldsymbol{P}^+ \bar{\boldsymbol{P}} + V_p U V_{\hat{p}} I_1, \qquad \text{where } I_1 = \begin{bmatrix} I_{\hat{n}_x} \\ 0 \end{bmatrix}$$

$$\hat{C} = P_0$$

$$\hat{D} = \boldsymbol{P}^+ \boldsymbol{M}_Q + V_p U V_{\hat{p}} I_2, \qquad \text{where } I_2 = \begin{bmatrix} 0 \\ W^{-1/2} \end{bmatrix}$$

$$\hat{H} = H_0$$

$I_{\hat{n}_x}$ is an I_{n_w} are identity matrix of dimension $\hat{n}_x$.

QMC from Arbitrary Inputs

Until now only pulse or white-noise inputs have been treated in the QMC theory. It is not difficult to extend the method to treat arbitrary inputs. We shall show the single-input case.

Note from Eq. (4) that

$$y(0) = H_0 w(0) \quad \text{or} \quad H_0 = y(0)w^{-1}(0)$$

$$y(1) = H_1 w(0) + H_0 w(1) \quad \text{or} \quad H_1 = [y(1) - H_0 w(1)]\, w^{-1}(0)$$

Hence, in general the Markov parameters can be computed recursively from the input-output data

$$H_k = \left(y_k - \sum_{i=0}^{k-1} H_i w_{k-i} \right) w^{-1}(0), \qquad k = 0,1,2,\ldots$$

Once the Markov parameters are computed in this way, the QMC algorithm can be applied to generate a QMC.

V. Minimast System Description and Identification Experiment

Located at the NASA Langley Research Center, the Minimast (see Fig. 1) is a deployable/retractable space truss with triangular cross section, which is representative of future trusses to be used in space. The total height of the truss is 21.6 m and it is cantilevered vertically from the base. This truss contains 18 bays in a single-laced configuration with every other bay repeating.

Two instrumented platforms have been installed at bay 10 and bay 18. Those actuators and sensors used for the control loop are all mounted on these two platforms. The configuration of these sensors and actuators is also shown in Fig. 1. The control inputs are three orthogonal torque wheel actuators (TWAx, TWAy, and TWAz) located on the platform at bay 18. Four accelerometers (A18X1, A18Y1, A18X2, A18Y2) are located at the tip platform 18, and the other two (A10X, A10Y) are located at the midplatform (bay 10). All accelerometers are mounted in either x or y directions for linear acceleration measurements. One rate gyro labeled R18z is mounted at the tip plate measuring the rotation rate about the x axis.

Nine displacement sensors are also used in our identification experiment (although they will not be used for feedback control). These are the Kaman proximity probes at bays 10, 14, and 18. Three Kaman proximity probes are installed at each bay. They are mounted parallel to the flat face on the corner joints of the structure and positioned to measure deflections normal to the face of the probe. The displacement sensors used are denoted D10A, D10B, D10C, D14A, D14B, D14C, D18A, D18B, D18C for the sensors at bays 10, 14, 18, and corners A, B, C.

Table 1 Definition of outputs of identification model

Output no.	Notation	Sensor	Location	
y_1	A18X1	Accelerometers	Bay 18	x axis
y_2	A18Y1	Accelerometers	Bay 18	y axis
y_3	A18X2	Accelerometers	Bay 18	x axis
y_4	A18Y2	Accelerometers	Bay 18	y axis
y_5	A10X	Accelerometers	Bay 10	x axis
y_6	A10Y	Accelerometers	Bay 10	y axis
y_7	R18Z	Rate gyro	Bay 18	z axis
y_8	D18A	Displacement sensor	Bay 18	Corner A
y_9	D18B	Displacement sensor	Bay 18	Corner B
y_{10}	D18C	Displacement sensor	Bay 18	Corner C
y_{11}	D14A	Displacement sensor	Bay 14	Corner A
y_{12}	D14B	Displacement sensor	Bay 14	Corner B
y_{13}	D14C	Displacement sensor	Bay 14	Corner C
y_{14}	D10A	Displacement sensor	Bay 10	Corner A
y_{15}	D10B	Displacement sensor	Bay 10	Corner B
y_{16}	D10C	Displacement sensor	Bay 10	Corner C

Table 2 Definition of inputs of identification model

Input no.	Notation	Actuator/disturbance source	Location	
w_1	TWAx	Torque wheel	Bay 18	x axis
w_2	TWAy	Torque wheel	Bay 18	y axis
w_3	TWAz	Torque wheel	Bay 18	z axis
w_4	SHA	Shaker	Bay 9	Corner A
w_5	SHB	Shaker	Bay 9	Corner B
w_6	SHC	Shaker	Bay 9	Corner C

Force disturbance signals applied to the structure originate from three 50-lb shakers (labeled as SHA, SHB, and SHC) attached at corners A, B, C of bay 9. A cable is attached vertically to the tip plate to off-load the 350 lb of the tip plate and the TWAs.

A NASTRAN finite element model for the Minimast structure has been created by NASA.[18] The analytical model, which is composed of 149 structural modes with natural frequencies less than 10 Hz and 29 state variables for sensor/actuator dynamics, can be compared (Tables 3 and 4) with our identified model, although the important comparison is with the test data (since the finite element model may be in substantial error).

A sampling frequency of 50 Hz is used throughout the analysis and experiment. The choice of this sampling frequency is mainly dictated by the online control computation delay time consideration.

The model presumed for the Minimast system is the linear equation (1) with unknown dimensions and parameters (A,C,D). The output y and input w of this model are defined in Tables 1 and 2. Output pulse responses were obtained by applying single-pulse signals at each of six input channels. The raw measurements of these responses were contaminated severely by high-frequency environmental noise and low-frequency drifts caused by wind gusts on the building. Therefore, 10 measurements were collected for each input channel. The output pulse response signals [applied one at a time to form $Y_l(d,i)$, Y_k in Eqs. (6)] were produced by averaging the 10 measurements and also truncating (clamping to 0 dB) the frequency components below 0.4 Hz.

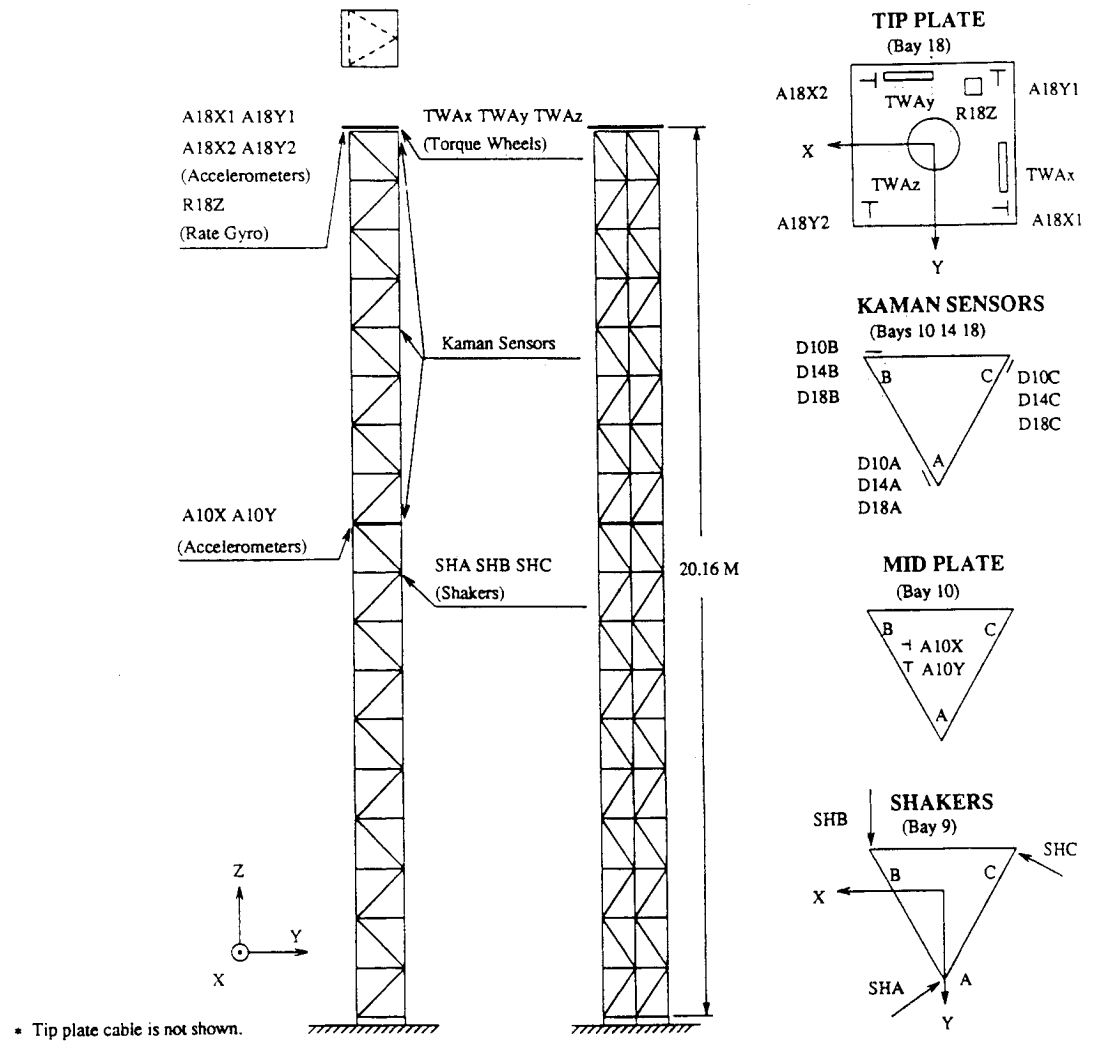

* Tip plate cable is not shown.

Fig. 1 Minimast ground test beam and sensor-actuator locations.

Twenty seconds of output pulse response ($d = 1000$) were collected for each input channel (after 20 s, the pulse-response measurements were below the noise level). We set $Q = 20$. For the total of 16 sensor outputs, this yields a square $\boldsymbol{D}_Q$ matrix of size 320 ($= 20 \times 16$).

Figure 2 shows 120 of the 320 singular values of the $\boldsymbol{D}_Q$ matrices computed in step 4 of the Q-Markov cover algorithm. Because of the substantial change in slope in Fig. 2 at singular value 18, the first 18 singular values are assumed to be the dominant singular values. A map of the identified model order and identified frequencies is shown in Fig. 3. These identified models are obtained by varying the zero threshold ϵ so that orders of the models change from 2 to 80 in step 4 (that is, truncating singular values of $\boldsymbol{D}_Q$, smaller than ϵ, yielding models of order 2 to 80). Table 3 shows the frequencies of NASA's finite element model (FEM) model below 25 Hz. Comparing the identified frequencies in Fig. 3 with the analytical frequencies in Table 3, we can see agreement on the first bending, second bending, and first torsion frequencies beginning at model order = 14 (in the FEM these modes also had the largest modal costs). Starting from model order 20, the identified models pick up more and more local frequencies. When the model order is higher than 20, the identified model begins to possess local frequencies occurring between frequency 10 and 20 Hz. Figure 4 shows the H_2 norm of the errors between the frequency response of the identified model and the measured frequency response (normalized by the H_2 norm of the measured frequency response). After model order 80, increasing model order does not reduce the error significantly. Table 4 compares the frequencies of a model of order $\hat{n}_x = 40$ and the

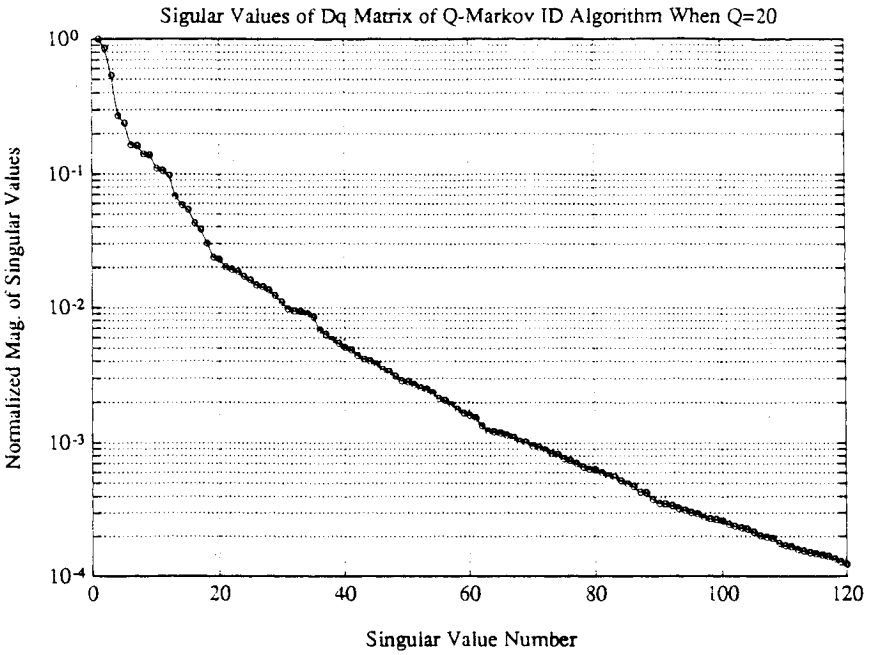

Fig. 2 Singular values of D_Q matrix of Q-Markov cover identification algorithm when $Q = 20$.

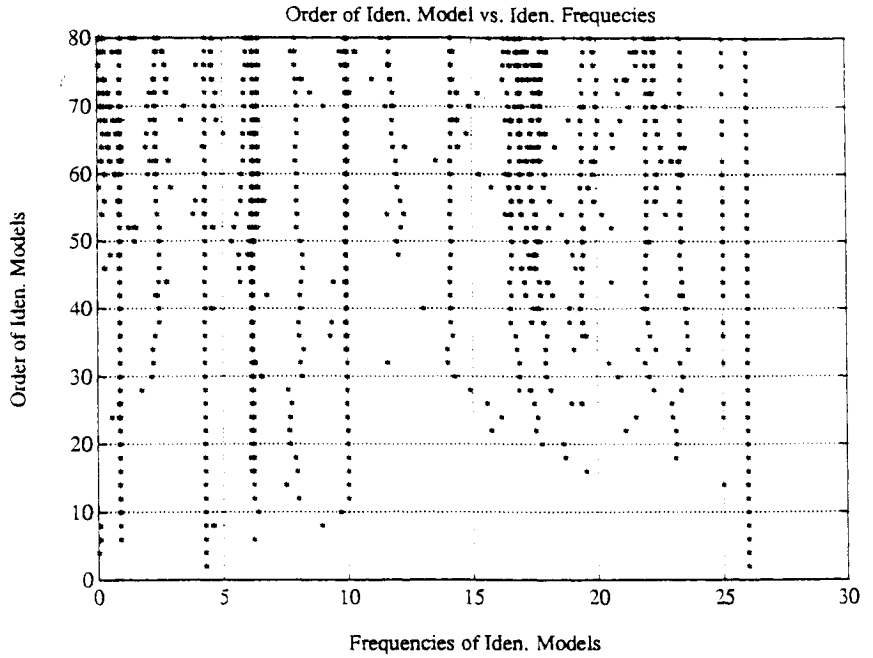

Fig. 3 Map of order of identified model vs identified frequencies.

Table 3 Frequencies of NASA's FEM model below 25 Hz

Mode no.	Description	Frequency, Hz
1	First bending (B1)	0.8010
2	First bending (B1)	0.8016
3	First torsion (T1)	4.3644
4	Second bending (B2)	6.1040
5	Second bending (B2)	6.1568
6–116	Local and cable modes	
117	Tip plate (TIP-1)	20.305
118	Second torsion (T2)	21.562
119	Tip plate with third bending (TIP-2/B3)	23.470

Table 4 Frequencies of identified 40th-order model and FEM model

$\hat{n}_X = 40$	FEM	Description
0.8613	0.8010	First bending
0.8829	0.8016	First bending
2.4165		
4.275	4.3644	First torsion
4.557		
6.1531	6.1040	Second bending
6.1633	6.1568	Second bending
6.2385		
8.1076		
9.9101	110	Local and
9.9464	Frequencies	cable modes
13.0174		
14.1066		
16.527		
17.435		
17.628		
18.870		
19.3118	20.305	Tip plate
21.8288	21.562	Second torsion
21.9303		
23.473	23.470	Tip plate with third bending

frequencies of the finite element model under 25 Hz. The finite element model is not presumed here to be a good model, but the comparison shows the difference between our results and those in Refs. 19 and 20.

VI. Identified 40th-Order Model and Control Design

In this section we present the identified model of order 40. Figures 5–8 compare the pulse responses and frequency responses of the identified model and the measured (laboratory) data. We believe that the measured data in Fig. 5 is very noisy, since there is essentially no damping after 12 s. The system responses in Figs. 5 and 6 are responses of the displacement sensors at bay 10 corner B (D10B) to the torque. The response shown in Figs. 7 and 8 is the response of the rate gyro to the torque. In the frequency response of the D10B to TWAx (Fig. 6), one can clearly see the first bending and second bending frequencies. For this response, bending dynamics play a dominant role. In the frequency response of the R18z to TWAz (Fig. 8), the first torsion frequency dominates the response, as expected. The pulse response of the identified model does not precisely match the first 20 pulse-response samples of measured pulse responses in Figs. 5 and 7 due to truncation of some nonzero singular values of the D_Q matrix (which the QMC theory does not allow). Nonetheless, by choosing Q, ϵ, and U (the free parameters), it is usually possible to get reasonable models. Future research should provide more precise ways of doing this to reduce the effects of measurement errors.

Based on our analysis of the identification results, the model of order 40 seems to be the best. The models with orders less than 40 do not represent the experimental data as well as the 40th-order model. Higher-order models seem to capture more noise characteristics in the experimental data.

Note that when pulses are applied through both control channels and disturbance channels, the $Dw(k)$ in Eqs. (1) becomes

$$[B \quad D]\begin{bmatrix} u(k) \\ w(k) \end{bmatrix}$$

and when identification measurements include both control outputs and measurements, the $Cx(k)$ in Eqs. (1) becomes

$$\begin{bmatrix} C \\ M \end{bmatrix} x(k)$$

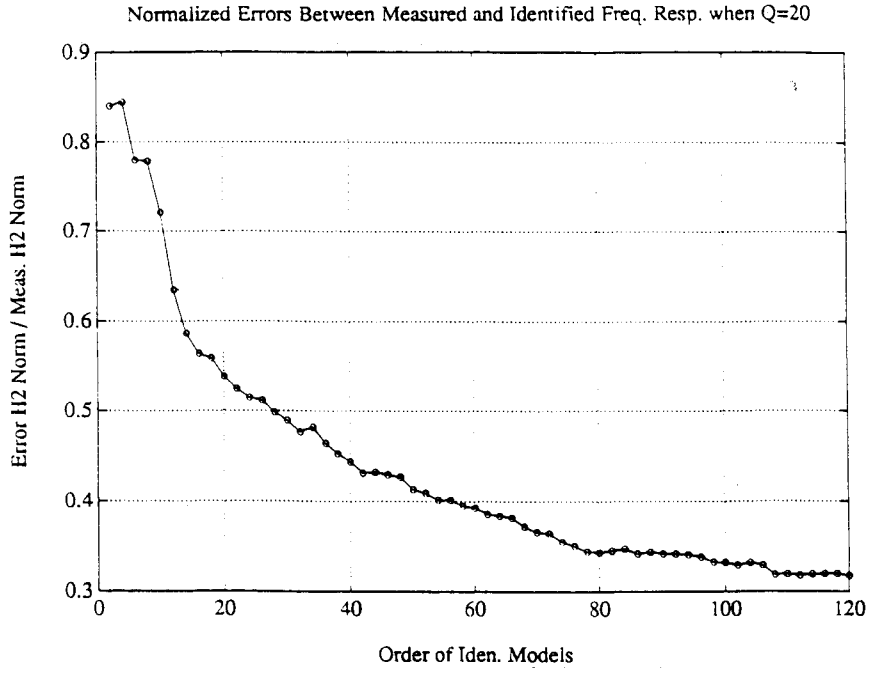

Fig. 4 Normalized errors between measured and identified frequency responses.

so that B, D, C, and M are identified for the control design model

$$\hat{x}_1(k+1) = \hat{A}\hat{x}(k+1) + \hat{B}u(k) + \hat{D}w(k)$$

$$\hat{y}(k) = \hat{C}\hat{x}(k)$$

$$z(k) = \hat{M}\hat{x}(k) + v$$

Outer Variance Constrained Controller Design: The identified 40th-order model was used to design a controller to reduce the vibration of Minimast.[19,20] The model for control design was reduced from 40 to 12 by the integrated model reduction and output variance constrained (OVC) control design algorithm,[19,22] producing a 12th-order controller. The OVC controller is designed to solve the following optimization problem:

Minimize

$$J = \lim_{k\to\infty} E\{u^*(k)Ru(k)\}$$

subject to

$$\lim_{k\to\infty} Ey_i^2(k) \le \sigma_i^2, \qquad i = 1,\ldots,n_y \tag{22}$$

where $u(k)$ is the control signal (applied at 50 Hz), R is the weighting matrix on the control effort, $y(k)$ is the vector output signal, and σ_i^2 is the constraint on the ith output variance.

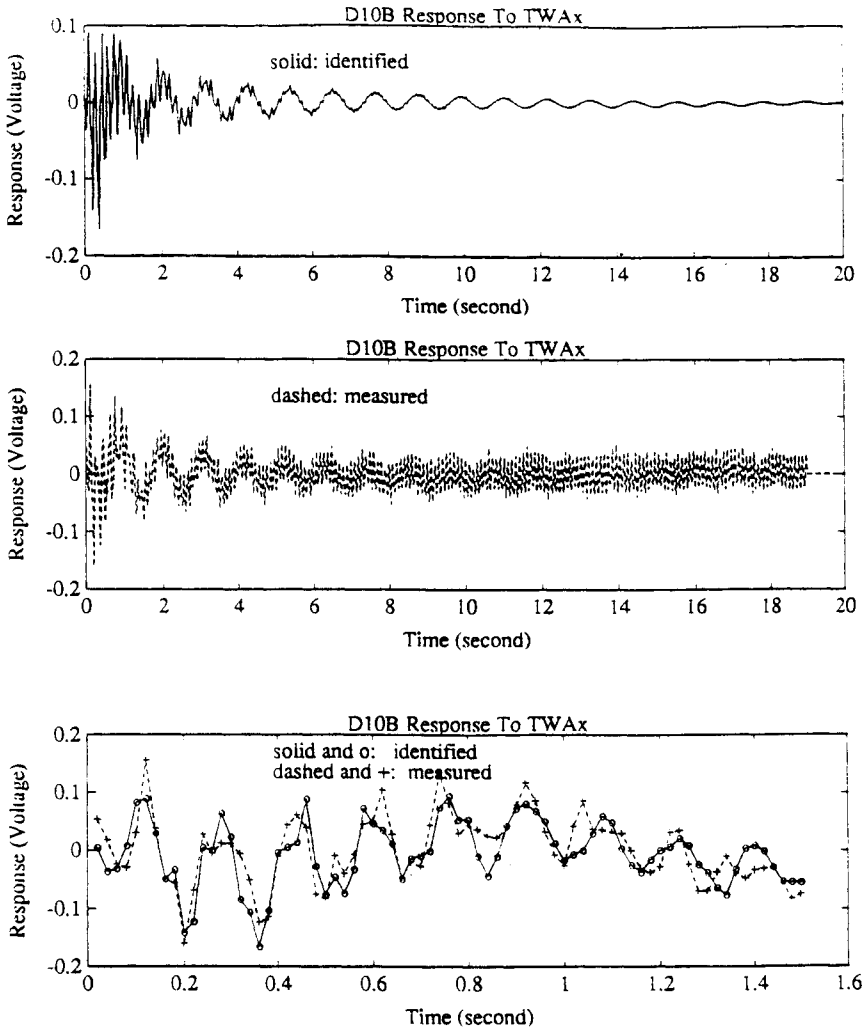

Fig. 5 Impulse responses of identified model and measured impulse response.

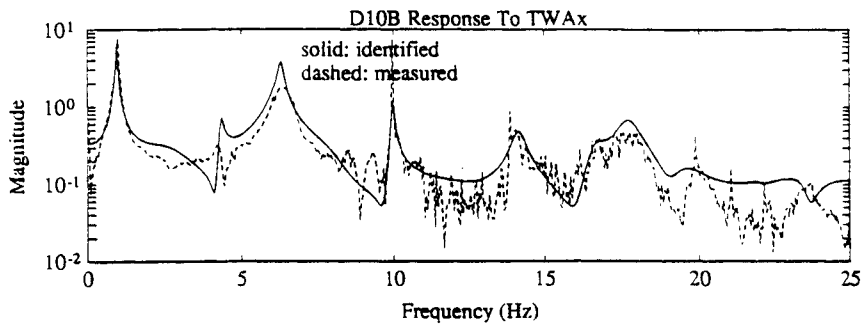

Fig. 6 Comparison of identified frequency response with measured data Fourier transform.

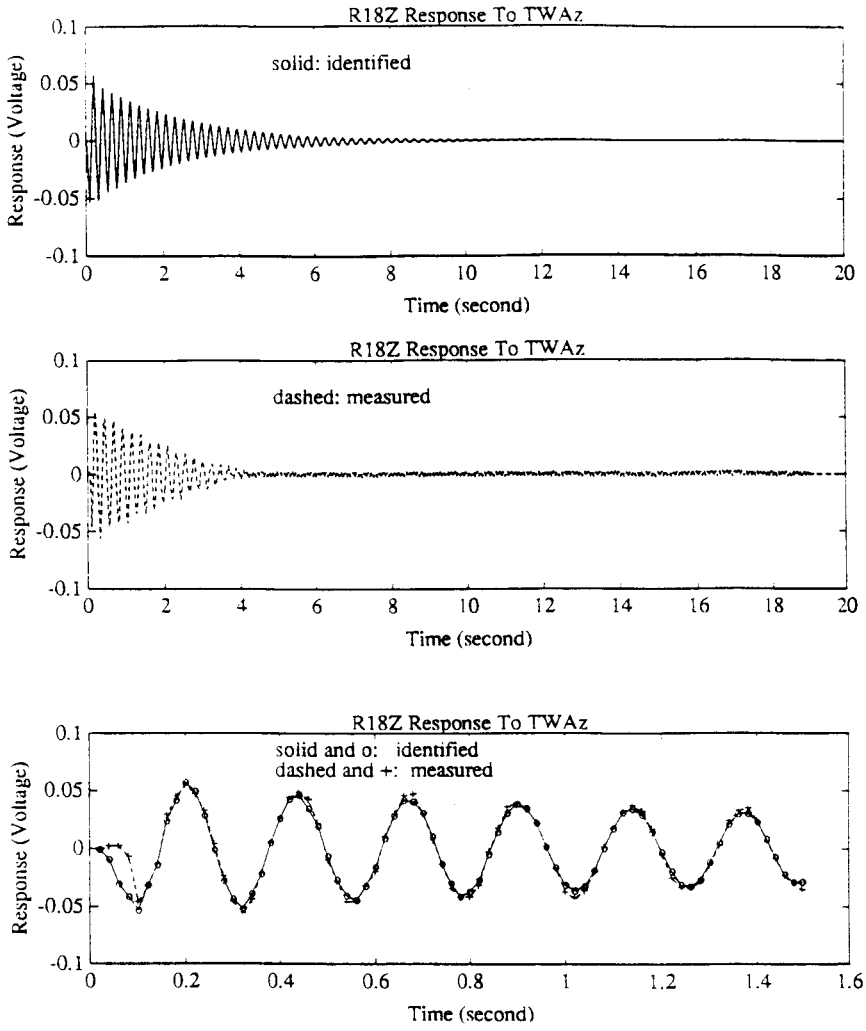

Fig. 7 Impulse responses of identified model and measured impulse response.

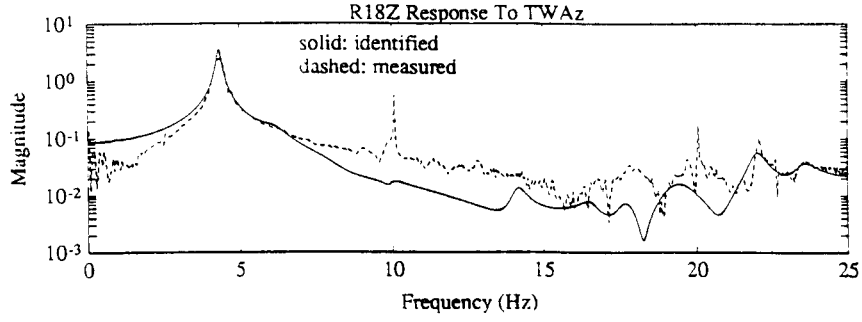

Fig. 8 Comparison of identified frequency response with measured data Fourier transform.

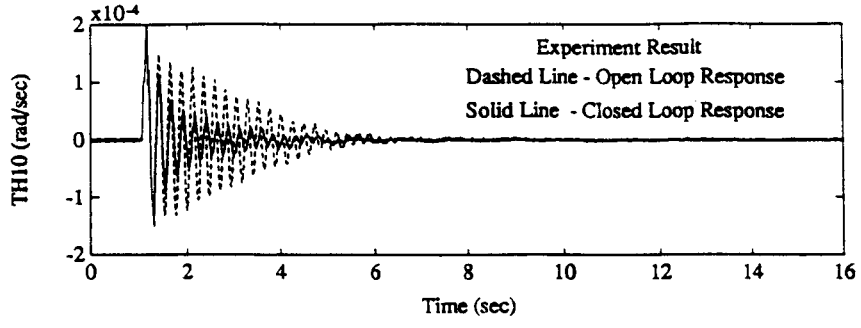

Fig. 9 Closed-loop impulse response of TH10 (case 3).

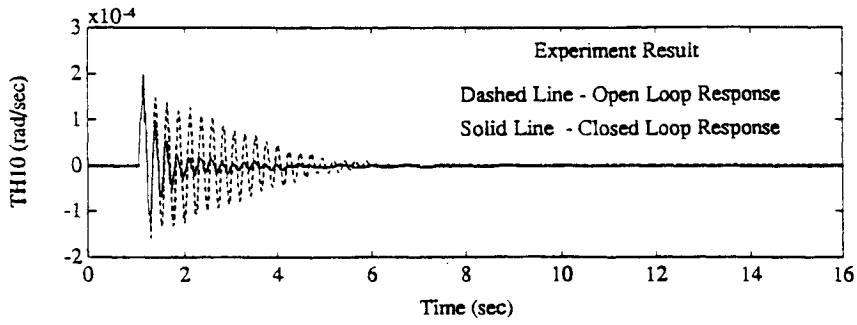

Fig. 10 Closed-loop impulse response of TH10 (case 2).

The modes chosen by the integrated algorithm to form a 12th-order reduced model are two identified first bending modes, two identified second bending modes, and the identified first and second torsion modes. The 12th OVC controller was designed by the algorithm based on this model. Further analysis after the design showed that lower-order controllers (order less than 12) would degrade the control performance and higher-order controllers would not improve the performance significantly.

Figure 9 shows the results of laboratory tests when the OVC controller is implemented on the Minimast. Figure 9 shows the response of the rotation angle of the structure at bay 10 to shaker A force. The closed-loop system controller is stable, and the vibration of the structure has been significantly reduced even in the presence of some nonlinearities. Note the effects of Coulomb friction in the open-loop response of the experimental tests, resulting in the linear decay in Figs. 7b, 9, and 10 (this is a feature of Coulomb friction[21]) rather than the exponential decay associated with the linear identified model in Fig. 7a. We point out that due to laboratory time limitations, this controller is the first (and only) attempt implemented on the Minimast from the identification model for controller design (without any on-site tuning of the controller). Figure 10 shows the laboratory test result of the 12th-order OVC controller design using the FEM, from Refs. 19 and 20. It shows the response of the rotation angle TH10 to shaker A force. Comparing the response in Figs. 9 and 10, we can see some difference between the controller designed by the identified model and the performance of the controller designed by the FEM. However, the FEM has been massaged for over a year to improve it. We believe that some tuning of the QMC model would improve Fig. 9 to the same level of performance as in Fig. 10. The very positive news here is the "black box" identification approaches such as the QMC can produce models for control design that are competitive with FEMs, given a sufficiently rich set of input/output measurements.

VII. Conclusions

This paper presents a new Q-Markov covariance equivalent realization algorithm for identification and applies it to a real flexible structure—NASA's Minimast. In the absence of measurement errors, the theory promises to generate all models which will match the first Q autocorrelations of the output and the pulse response up to time $k = Q - 1$. Other features of the theory include the preservation of nonminimal-phase properties, preservation of the output covariance matrix, and the guarantee of stability and minimality (observability and controllability).

The new algorithm produces Q-Markov covariance equivalent realizations from either pulse responses or white-noise responses, whereas prior Q-Markov covariance equivalent realization algorithms required both pulse and white-noise responses.

In the presence of measurement noise, it is advisable to set zero threshold ϵ to some numerically nonzero values for the rank test, even though this will lead to some mismatch in the Markov and covariance parameters. How to choose this threshold ϵ, the number Q, and the arbitrary unitary matrix that parameterizes all Q-Markov covariance equivalent realizations of the system, remain open questions for interesting future research.

The Q-Markov covariance equivalent realization algorithm identified all of the dominant modes of the Minimast structure, and the controller designed based on this model produced performance similar to that achieved by controller design using finite element models of the system. The finite element models were tuned and improved over a long period of time, whereas the identified model and subsequent controller design were first attempts. Hence, this report has not had the benefit of tuning either the identified models or the controller in laboratory tests. The test results of Q-Markov covariance equivalent realization identification are therefore very encouraging.

Acknowledgments

This work was sponsored by NASA Grant NAG1-958. Thanks go to our technical monitors, S. Joshi, R. Pappa, and R. Taylor, and to those who provided technical support in the Minimast laboratory, J. Sulla, S. Perez, and Z. Kim. We gratefully acknowledge also the help of C. Hsieh and J. Kim, who performed the laboratory experiments and collected the data.

References

[1]Ho, B. L., and Kalman, R. E., "Effective Construction of Linear State-Variable Models From Input Output Data," *Regelungstechnik,* Vol. 14, 1966, pp. 152–192.

[2]Kung, S., "A New Identification and Model Reduction Algorithm Via Singular Value Decompositions," 12th Asilomar Conference on Circuits, Systems, and Computers, Pacific Grove, CA, Nov. 1978.

[3]Juang, J. N., and Pappa, R. S., "An Eigensystem Realization Algorithm for Modal Parameter Identification and Model Reduction," *Journal of Guidance, Control, and Dynamics,* Vol. 8, No. 5, 1985, pp. 620–627.

[4]Juang, J.-N., Cooper, J. E., and Wright, J. R., "An Eigensystem Realization Algorithm Using Data Correlations (ERA/DC) For Modal Parameter Identification," *Control-Theory and Advanced Technology,* Vol. 4, No. 1, 1988, pp. 5–14.

[5]Boram, Y., and Porat, B., "Identification of Minimal Order State Space Models From Stochastic Input-Output Data," *SIAM Journal of Control and Optimization,* Vol. 26, 1988, pp. 56–65.

[6]Tugnait, J. K., "Order Reduction of SISO Nonminimum-Phase Stochastic Systems," *IEEE Transactions on Automatic Control,* Vol. AC-31, July 1986, pp. 623–632.

[7]Rissanen, J., and Kailath, T., "Partial Realization of Random Systems," *Automatica,* Vol. 8, 1972, pp. 389–396.

[8]Dickinson, B., Morf, M., and Kailath, T., "A Minimal Realization Algorithm for Matrix Sequences," *IEEE Transactions on Automatic Control,* Vol. AC-19, 1974, pp. 31–38.

[9]Anderson, B. D. O., "The Inverse Problem of Stationary Covariance Generation," *Journal of Statistical Physics,* Vol. 1, 1969, pp. 133–147.

[10]Mullis, C. T., and Roberts, R. A., "The Use of Second-Order Information in the Approximation of Discrete-Time Systems," *IEEE*

Transactions on Acoustics, Speech, Signal Processing, Vol. ASSP-24, No. 3, 1976, pp. 265.

[11]Inouye, Y., "Approximation of Multivariable Linear Systems with Impulse Response and Autocorrelation Sequences," *Automatica,* Vol. 19, No. 3, 1983, p. 265.

[12]Yousuff, A., Wagie, D. A., and Skelton, R. E., "Linear System Approximation Via Covariance Equivalent Realization," *Journal of Mathematical Analysis and Applications,* Vol. 106, No. 1, 1985, pp. 91–115; also "A Projection Approach for Model Reduction By Matching Output Covariances and Markov Parameters," *22nd IEEE CDC,* Session WP1 (San Antonio, TX), Dec. 1983.

[13]Wagie, D. A., and Skelton, R. E., "A Projection Approach to Covariance Equivalent Realizations of Discrete Systems," *IEEE Transactions on Automatic Control,* Vol. AC-31, 1986, p. 1114.

[14]Anderson, B. D., and Skelton, R. E., "Generation of All q-Markov Covers," *IEEE Transactions on Circuits and Systems,* Vol. 35, No. 4, 1988, pp. 375–384.

[15]King, A. M., Desai, U. B., and Skelton, R. E., "A Generalized Approach to q-Markov Covariance Equivalent Realizations of Discrete Systems," *Automatica,* Vol. 24, No. 4, 1988, pp. 507–515.

[16]Skelton, R., *Dynamic Systems Control,* Wiley, New York, 1988.

[17]Glover, K., "All Optimal Hankel Norm Approximations of Linear Multivariable Systems and Their L_∞ Error Bound," *International Journal of Control,* Vol. 39, No. 6, 1984, pp. 1115–1193.

[18]Pappa, R., Sulla, J., et al., "Mini-Mast CSI Testbed—User's Guide," NASA Langley Research Center, Hampton, VA, March 23, 1989.

[19]Hsieh, C., Kim, J. H., Liu, K., Zhu, G., and Skelton, R. E., "Control of NASA's Minimast—An Approach Integrating Modeling and Control," *NASA Guest—Investigator Program Annual Report,* Purdue Univ., West Lafayette, IN, 1990.

[20]Hsieh, C., Kim, J. H., Zhu, G., Liu, K., and Skelton, R. E., "An Iterative Algorithm Combining Model Reduction and Control Design," *Proceedings of the 1990 American Control Conference* (San Diego, CA), May 1990.

[21]Chapman, J. M., Shaw, F. H., and Russell, W. C., "Nonlinear Transient Anlaysis of Joint Dominated Structures," AIAA Paper 87-0892, April 1987; also presented by J. M. Chapman (Boeing Aerospace and Electronics, Seattle) at the CSI-GI Program Mid-Year Review, NASA Langley Research Center, Hampton, VA, July 11, 1989.

[22]Liu, K., "Q-Markov Cover Identification and Integrated MCA-OVC Controller Design for Flexible Structures," Ph.D. Dissertation, School of Aeronautics and Astronautics, Purdue Univ., West Lafayette, IN, Dec. 1991.